How to cite: *Angew. Chem. Int. Ed.* **2024**, *63*, e202412417
doi.org/10.1002/anie.202412417

Iron Porphyrins | Hot Paper

Operando Spectroelectrochemistry Unravels the Mechanism of CO_2 Electrocatalytic Reduction by an Fe Porphyrin

Aude Salamé, Mun Hon Cheah, Julien Bonin, Marc Robert,* and Elodie Anxolabéhère-Mallart**

Abstract: Iron porphyrins are molecular catalysts recognized for their ability to electrochemically and photochemically reduce carbon dioxide (CO_2). The main reduction product is carbon monoxide (CO). CO holds significant industrial importance as it serves as a precursor for various valuable chemical products containing either a single carbon atom (C1), like methanol or methane, or multiple carbon atoms (Cn), such as ethanol or ethylene. Despite the long-established efficiency of these catalysts, optimizing their catalytic activity and stability and comprehending the intricate reaction mechanisms remain a significant challenge. This article presents a comprehensive investigation of the mechanistic aspects of the selective electroreduction of CO_2 to CO using an iron porphyrin substituted with four trimethylammonium groups in the *para* position $[(pTMA)Fe^{III}–Cl]^{4+}$. By employing infrared and UV/Visible spectroelectrochemistry, changes in the electronic structure and coordination environment of the iron center can be observed in real-time as the electrochemical potential is adjusted, offering new insights into the reaction mechanisms. Catalytic species were identified, and evidence of a secondary reaction pathway was uncovered, potentially prompting a re-evaluation of the nature of the catalytically active species.

[*] A. Salamé, Prof. J. Bonin, Prof. M. Robert, Dr. E. Anxolabéhère-Mallart
Laboratoire d'Electrochimie Moléculaire (LEM)
Université Paris Cité
FF-75013 Paris, France
E-mail: robert@u-paris.fr
elodie.anxolabehere@u-paris.fr

Dr. M. Hon Cheah
Molecular Biomimetics, Department of Chemistry—Ångström
Uppsala University
751 20 Uppsala, Sweden
E-mail: michael.cheah@kemi.uu.se

Prof. M. Robert
Institut Universitaire de France (IUF)
F-75005 Paris, France

Introduction

The electrochemical catalytic reduction of carbon dioxide (CO_2) to carbon monoxide (CO, the most commonly obtained product) by molecular catalysts is no longer receiving the same level of attention as before. This observation indicates the advancement made on CO_2 reduction reactions (CO_2RR) in the last years. Albeit rare, new molecular based electrocatalytic systems able to reduce CO_2 with 6 (CH_3OH) or 8 (CH_4) electrons, as well as to small amount of C2+ products, recently emerged.[1–4] However, the generation of CO is still of great interest as it is an essential building block in organic and inorganic synthesis, as well as an important intermediate in electro- and photochemical catalytic CO_2RR towards C1 and/or more reduced C2+ products.[1,5–11]

Iron porphyrins are a class of molecular catalysts well-known since early works in the 1980s for their efficiency and selectivity towards CO production.[12–21] Despite numerous studies to clarify the mechanism of the electro- and photochemical CO_2 reduction to CO catalyzed by these complexes, there are still a number of grey areas. Typical approaches to investigate such an electron-induced mechanism include both: (1) cyclic voltammetry (CV), the modification of the scan rate providing valuable information on the mechanism, on kinetics of the catalytic process, and on product formed during catalysis; and (2) spectroelectrochemistry (SEC),[22,23] which allows characterizing a given oxidation state and coordination sphere of the catalyst by a specific spectroscopic signature. Among all the spectroscopic techniques available, X-ray absorption (XAS),[24–27] Fourier transform infrared spectroscopy (FTIR)[28,29] and UV/Visible[18,26,30] SEC have already been used to decipher the mechanism of homogeneous catalytic CO_2RR systems. In this work, FTIR and UV/Visible SEC were used *in situ* and operando to highlight the coordination of CO to the Fe^X metal center of the porphyrin (X denoting the formal metal oxidation state III, II, I, or 0). Capturing such reaction intermediates is crucial for understanding the reactivity involved in the electrochemical reduction of CO_2 to CO. The use of SEC could also enhance the identification of potential side reactions involving the porphyrin ligand when the catalyst reaches highly reduced states, particularly the catalytically active Fe^0 state. Modifications affecting the porphyrin ring following the transfer of multiple electrons can be partially explained by the delocalization of electrons from the iron center to the ligand.[27,31,32] This induces polarization of the porphyrin ligand and renders it more

susceptible to additional side reactions, *e.g.* protonation, as will be explained in the following.

Previous research focused on understanding the mechanism of homogeneous CO_2 electrocatalysis to CO by iron porphyrins using SEC as a tool.[26,34–37] Notably, our group studied the homogeneous [(TPP)Fe^{III}–Cl] model system (iron tetraphenylporphyrin with the non-functionalized ring) by *in situ* and operando XAS and UV/Visible SEC in the absence of added proton source (Scheme 1A).[26] Two types of interactions between CO_2 and the catalyst were identified: (i) the coordination of CO_2 to the iron center of the triply reduced species [(TPP)Fe^{III}–Cl]+3e$^-$) and (ii) a weaker interaction between CO_2 and the doubly reduced species ([(TPP)Fe^{III}–Cl]+2e$^-$). This study confirms previous results showing that the rate determining step of the catalysis was the breaking of one C–O bond of CO_2.[38] Additionally, Deeba *et al.* employed UV/Visible and EPR SEC techniques with [(TPP)Fe^{III}–Cl] catalyst to demonstrate that the resting state of the catalyst was the [(TPP)Fe^{I}]$^-$ species.[34]

To go deeper in the understanding of the catalytic mechanism, this article focuses on the electrocatalytic activity of a modified iron porphyrin that has been introduced by our group, *i.e.* the meso-tetra(4-N,N,N-trimethylanilinium) iron (III) porphyrin tetrachloride, (Scheme 1B, quoted as [(pTMA)Fe^{III}–Cl]$^{4+}$ in the following).[31,39–43]

Its metrics for the electro- and photo-catalytic reduction of CO_2 to CO in organic solvents[39,42] and water[41,43] have previously been reported, reaching nearly 100 % Faradaic efficiency (FE) and selectivity towards CO for several hours. The high activity of this catalyst has been attributed to through-space substituent effects which stabilize the Fe^0–CO_2 adduct thanks to coulombic interactions with the partial negative charge developing onto the oxygen atoms upon CO_2 binding at the Fe center.[42] The catalytic rate for CO production in electrochemical conditions was inferred from cyclic voltammetry analysis, however a comprehensive mechanistic study is lacking.[42,43]

Herein, we present a detailed experimental mechanistic investigation on the high-pressure electrochemical reduction of CO_2 to CO, catalyzed by [(pTMA)Fe^{III}–Cl]$^{4+}$ in DMF/$TBAPF_6$ medium. This study was conducted by working under a CO_2 partial pressure of 3 bars using a pressurized thin-layer spectroelectrochemical cell.[44] By employing a combination of scanning SEC techniques, allowing *in situ* UV/Visible and FTIR spectra collection during a cyclic voltammetry scan, along with conventional cyclic voltammetry, we successfully characterized both carbonyl and non-carbonyl intermediates involved in the CO_2-to-CO reduction reaction. Additionally, we identified side reactions occurring at the pTMA ligand when binding CO to the highly-reduced Fe^0 state.

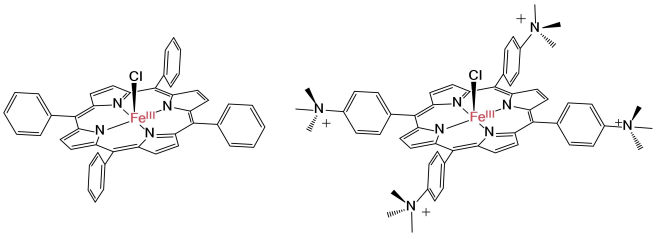

Scheme 1. Structure of the [(TPP)Fe^{III}–Cl] (A) and [(pTMA)Fe^{III}–Cl]$^{4+}$ (B) molecular catalysts.

Results and Discussion

Spectroelectrochemistry of (pTMA)Fe under Ar Atmosphere

Cyclic voltammetry (CV) coupled to UV/Visible spectroelectrochemistry (UV/Vis SEC) carried out under argon atmosphere (Figure 1) first provided insights into oxidation states and coordination environment of the catalyst at various potentials. At open circuit potential (OCP, dark blue dot, Figure 1A and dark blue spectrum,

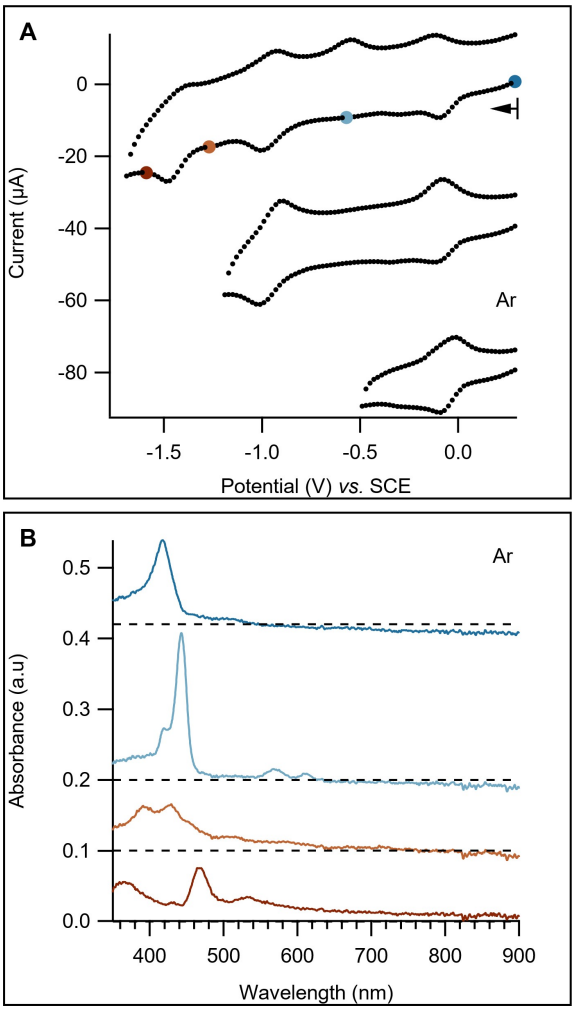

Figure 1. UV/Vis SEC under 1 bar Ar atmosphere, [(pTMA)Fe^{III}–Cl]$^{4+}$ 0.5 mM in DMF/0.1 M $TBAPF_6$. A: CV collected during scanning SEC, scan rate 20 mV/s. B: Representative spectra obtained at various electrode potential E *vs.* SCE. (Dark blue) E = +0.15 V ([(pTMA)Fe^{III}–Cl])$^{4+}$. (Light blue) E = −0.55 V ([(pTMA)Fe^{II}–Cl]$^{3+}$). (Orange) E = −1.25 V ([(pTMA)Fe^{I}]$^{3+}$). (Red) E = −1.55 V ([(pTMA)Fe^{0}]$^{2+}$).

Figure 1B) the stable species is $[(pTMA)Fe^{III}–Cl]^{4+}$. A broad absorption Q band around 380 nm is observed, similar to the one reported in the case of $[(TPP)Fe^{III}–Cl]$ and attributed to an iron-to-chloride-charge-transfer transition, which signs the coordination of one Cl^- as axial ligand to the Fe^{III} center.[45]

Similar coordination is expected for $[(pTMA)Fe^{III}–Cl]^{4+}$ in DMF/$TBAPF_6$. After reduction at −0.6 V *vs.* SCE, a new spectrum is observed (light blue dot on CV, Figure 1A and light blue spectrum, Figure 1B) which we attributed to the singly reduced form $[(pTMA)Fe^{II}–Cl]^{3+}$. The coordination of chloride ion at the Fe^{II} species is discussed in the Supporting Information (Figure S1). After reduction at −1.3 V *vs.* SCE, a new spectrum is obtained (orange dot on CV, Figure 1A and orange spectrum, Figure 1B) and is assigned to the formation $[(pTMA)Fe^{I}]^{3+}$ based on the similar spectrum reported for $[(TPP)Fe^{I}]^-$.[26] A third electron transfer at −1.55 V *vs.* SCE finally resulted in the formation of the formal $[(pTMA)Fe^{0}]^{2+}$ species (red dot on CV, Figure 1A and red spectrum, Figure 1B) which has been shown to be the catalytically active species towards CO_2 reduction (Figure S2A).[12] This third reduction process is irreversible and related to the appearance of a new re-oxidation peak (−0.6 V *vs.* SCE), indicating the presence of a chemical reaction impacting $[(pTMA)Fe^{0}]^{2+}$. Alkylation of Fe^0 with the electrolyte cation TBA^+ has been reported in the literature on multiple occasions, notably with the (TPP)Fe complex.[46,47] However $[(pTMA)Fe^{0}]^{2+}$ species does not react with the TBA^+ cation from our DMF/$TBAPF_6$ supporting electrolyte. Indeed, similar irreversibility and re-oxidation peaks (−0.6 V *vs.* SCE) were observed on the CV recorded in the same conditions with $NaClO_4$ as the supporting electrolyte (Figure S3), thus ruling out the alkylation reaction by TBA^+. Qualitatively, the absence of alkylation reaction can be rationalized by electrostatic repulsion between the doubly positively charged iron complex and the TBA^+ cation. The exact chemical reaction involving $[(pTMA)Fe^{0}]^{2+}$ will be further explained. The formal writing of the Fe^0 state in which the electronic density is localized on the metal can be represented by two mesomeric forms, $[(\bullet pTMA)Fe^{I}]^{2+}$ and $[(\bullet\bullet pTMA)Fe^{II}]^{2+}$. "•" relates to electronic density being localized onto the porphyrin ligand. Experimentally, the consequence of such partial localization of the electron density results in an increase in the ligand's basicity, making it more prone to chemical reaction such as protonation. Two specific positions of the ligand, namely the carbon atoms located in the *meso* and *beta* positions of the porphyrin ligand are thus susceptible to protonate (Scheme S1). These possible protonations of the ligand would produce unique UV/Visible signatures,[48] making this technique very useful for their detection. Collecting these SEC UV/Vis signatures for each reduced state of $[(pTMA)Fe^{III}–Cl]^{4+}$ under Ar atmosphere will prove to be useful for systematic comparison when the coordination environment at the Fe center changes.

In order to investigate the phenomena involved in the catalytic CO_2RR, it is critical to find a technique allowing the direct detection and identification of possible intermediates such as Fe–CO or Fe–COH. FTIR SEC is a very sensitive method able to detect C=O bond vibrations ($\nu_{C=O}$) of metal carbonyl species, thanks to the high polarization of the bond. We scrutinized the $\nu_{C=O}$ IR region from 1800 to 2000 cm^{-1} for all the following FTIR SEC experiments carried out in DMF/$TBAPF_6$ medium.

FTIR Spectroelectrochemistry under CO_2 Atmosphere

Operando FTIR SEC experiments were carried out under a CO_2 partial pressure (P_{CO2}) of 3 bars without the addition of a proton source (Figure 2). A high CO_2 pressure was used in order to increase its concentration in solution and therefore enhance catalysis. In this case, CO_2 is reduced to CO by the transfer of an oxygen atom to a second molecule of CO_2, acting as a Lewis acid, therefore producing a carbonate species (CO_3^{2-}).[12] The corresponding CV exhibited a peak-

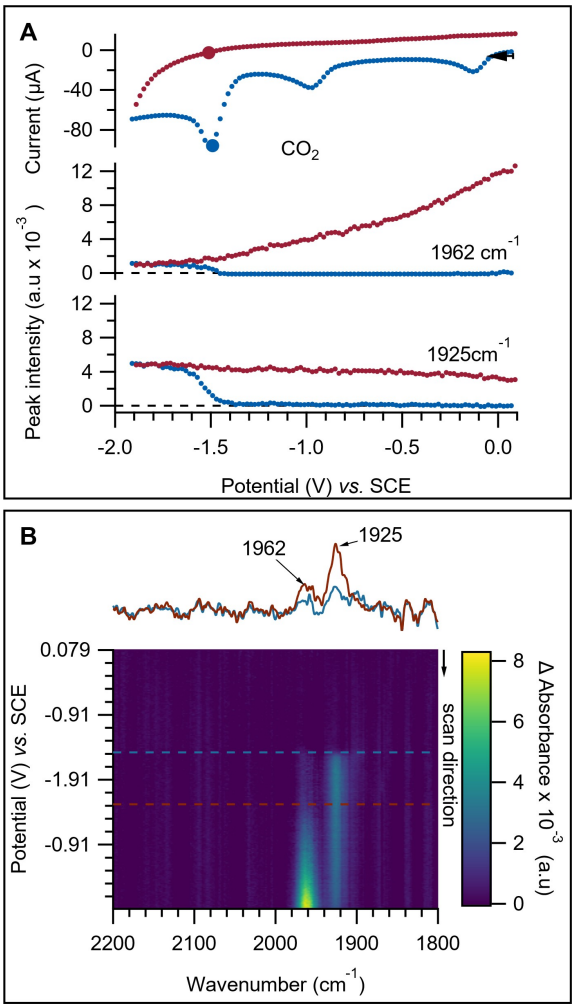

Figure 2. FTIR SEC under 3 bars CO_2 atmosphere, $[(pTMA)Fe^{III}–Cl]^{4+}$ 0.5 mM in DMF/0.1 M $TBAPF_6$. A, top: CV data collected during scanning SEC, scan rate 20 mV/s; bottom: estimated peak intensity of band at 1962 cm^{-1} and 1925 cm^{-1}. B, top: IR spectra collected at −1.51 V *vs.* SCE, color coded according to highlights in top panel; bottom: False color image representation of spectral changes during scanning SEC.

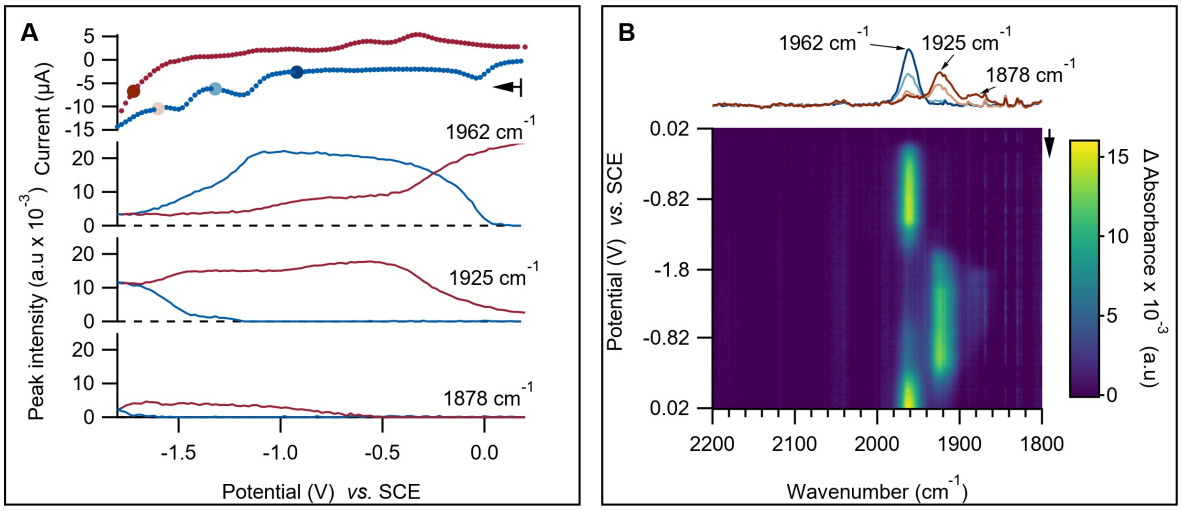

Figure 3. FTIR SEC under a CO atmosphere of 3 bars, $[(pTMA)Fe^{III}–Cl]^{4+}$ 0.5 mM in DMF/0.1 M $TBAPF_6$. A, top: CV data collected during scanning SEC, scan rate 18 mV/s; bottom: peak intensity of 1962, 1925 and 1878 cm^{-1} bands during SEC scan. B, IR spectra collected at corresponding color coded highlights in CV at top panel; bottom: False color image representation of spectral changes during scanning SEC.

shaped catalytic current starting −1.35 V *vs.* SCE on the forward scan, pointing to inhibition of the electrode surface by CO_3^{2-} deposition and therefore of catalysis at longer timescale.[14] However, it does not affect the detection of catalytically involved species. The FTIR spectra revealed the presence of two $\nu_{C=O}$ bands located at 1962 and 1925 cm^{-1}, respectively, which implies the formation of two Fe–CO species under catalytic conditions. The intensity of the 1962 cm^{-1} band remained very low during the forward scan and gradually increased during the reverse scan. Meanwhile, the intensity of the 1925 cm^{-1} band reached a maximum just after the peak potential of the catalytic wave and kept relatively constant during the reverse scan. Notably, there were no observable Fe–CO species prior to onset of catalysis at the third reduction wave. To allow the attribution of these two bands, FTIR SEC under CO atmosphere was performed to uncover the CO binding to the different oxidation states of $[(pTMA)Fe^{III}–Cl]^{4+}$catalyst.

FTIR Spectroelectrochemistry under CO Atmosphere

Under a CO partial pressure (P_{CO}) of 3 bars (Figure 3), three FTIR bands were observed. A high CO pressure was used in order to increase its concentration in solution and favor its coordination to the $[(pTMA)Fe^{III}–Cl]^{4+}$ complex. These three bands appear at 1962, 1925 and 1878 cm^{-1}, respectively, upon scanning from +0.2 to −1.8 V *vs.* SCE. The band at 1962 cm^{-1} was formed during the first reduction wave around −0.04 V *vs.* SCE (Figures S4A, B). Considering the high affinity of the Fe^{II} state for CO (Figure S2B) and the multiple reports of IR studies regarding this species[18,36] we attributed this band to the $[(pTMA)Fe^{II}–CO]^{4+}$ species. It is worth noting that this $[(pTMA)Fe^{II}–CO]^{4+}$ species was also detected at OCP due to partial photoreduction of the parent complex $[(pTMA)Fe^{III}–Cl]^{4+}$ under CO atmosphere. See Supporting Information for further discussion (Figure S5). The intensity of this band at 1962 cm^{-1} persisted until the potential reached the second reduction process (*ca.* −1.20 V *vs.* SCE) which corresponds to the reduction of Fe^{II} to Fe^{I}, after which it slowly began to decrease (light blue dot CV, Figure 3A, light blue spectrum, Figure 3B top and change of color intensity on pseudo color image, Figure 3B bottom, Figure S4C, D). Notably, the decrease in intensity of the 1962 cm^{-1} band was not correlated with the appearance of a new band. This experimental observation supports the reduction of $[(pTMA)Fe^{II}–CO]^{4+}$ to $[(pTMA)Fe^{I}–CO]^{3+}$ which was however not detected as evidenced by the lack of any other observable Fe–CO species in the $\nu_{C=O}$ region. CO de-coordinates from $[(pTMA)Fe^{I}–CO]^{3+}$ to form $[(pTMA)Fe^{I}]^{3+}$ species (Scheme 2).[33,34] The decarbonylation equilibrium between $[(pTMA)Fe^{I}]^{3+}$ and $[(pTMA)Fe^{I}–CO]^{3+}$ was further explored upon performing simulations of surface concentration profiles (Figure S7), showing that the formation of $[(pTMA)Fe^{I}]^{3+}$ was indeed favored and that the concentration of $[(pTMA)Fe^{I}–CO]^{3+}$ remained below the detection limit of FTIR.

At the third reduction wave (ca. −1.5 V vs. SCE), which corresponds to reduction of $[(pTMA)Fe^{I}]^{3+}$ into $[(pTMA)Fe^{0}]^{2+}$, a new band increased in intensity at 1925 cm^{-1}. While it is convenient to attribute this band to the formation of $[(pTMA)Fe^{0}–CO]^{2+}$, both our scanning SEC data and available literature do not support such assignment. First, the formation rate of the 1925 cm^{-1} band

$$[(pTMA)Fe^{I}]^{3+} + e^- \rightleftharpoons [(pTMA)Fe^{0}]^{2+}$$

$$[(pTMA)Fe^{0}]^{2+} + 2\,CO_2 \longrightarrow [(pTMA)Fe^{II}\text{-}CO]^{4+} + CO_3^{2-}$$

$$[(pTMA)Fe^{II}\text{-}CO]^{4+} + e^- \longrightarrow [(pTMA)Fe^{I}]^{3+} + CO$$

Scheme 2. Global mechanism of CO_2 electroreduction to CO catalyzed by $[(pTMA)Fe^{III}–Cl]^{4+}$.

was not strongly correlated to the peak reduction current (Figure S8), in contrast with the response obtained for the 1962 cm^{-1} band for which appearance was correlated to the corresponding peak reduction current. Second, additional scan rate and CO partial pressure dependence studies (Figure S9) suggested a slow formation of the 1925 cm^{-1} band (in the order of s^{-1}), with a dependence on the partial pressure of CO. Third, analysis of the CV obtained during SEC under Ar atmosphere (Figure 4A, black) depicted irreversibility of the third reduction process (Fe^{I} conversion to Fe^{0})) and the appearance of a new re-oxidation peak (ca. −0.6 V vs. SCE) (Figure S10A) as well as additional features on the UV/Vis spectrum (Figure S10B), including a band at 430 nm and a wide band between 600 and 800 nm. These observations pointed towards the formation of a daughter product of $[(pTMA)Fe^{0}]^{2+}$ under SEC experiment conditions. A likely candidate is the phlorin anion $[H(\bullet pTMA)Fe^{II}]^{3+}$[48] (Scheme S2) since the basic porphyrin dianion (mesomeric form $[(\bullet\bullet pTMA)Fe^{II}]^{2+}$) is susceptible to ligand protonation from residual water present in DMF. This hypothesis was further corroborated by the electrogeneration of the phlorin species under Ar atmosphere at E = −2.1 V *vs.* SCE (see Supporting Information), followed by its characterization by cyclic voltammetry (Figure S11). This resulted in the identification of a green solution, characteristic of a protonated porphyrin ligand.[19,49,50] As a consequence, we propose that the species corresponding to the 1925 cm^{-1} absorption band is the adduct between the phlorin anion $[H(\bullet pTMA)Fe^{II}]^{3+}$ and CO.

UV/Visible Spectroelectrochemistry under CO_2 and CO Atmosphere

In order to characterize the species resulting from reaction between the phlorin anion $[H(\bullet pTMA)Fe^{II}]^{3+}$ and CO, we conducted additional investigation using UV/Vis SEC (Figure 4).

The spectra obtained under CO atmosphere by applying a potential E = −1.35 V *vs.* SCE, corresponding to the second reduction wave, showed high similarity to the one obtained under Ar atmosphere. This observation is consistent with FTIR SEC data described above, *viz.* reduction of $[(pTMA)Fe^{II}–CO]^{4+}$ to $[(pTMA)Fe^{I}–CO]^{3+}$ results in decarbonylation to form $[(pTMA)Fe^{I}]^{3+}$.

The spectra obtained under CO atmosphere by further reducing to a potential of −1.55 V *vs.* SCE (third reduction wave) led to significant spectral changes relative to that obtained under Ar atmosphere.

Specifically, a broad band centered at 858 nm was observed. Previous electrochemical and SEC studies on zinc tetraphenylporphyrin $[(TPP)Zn^{II}]$,[48] which is of interest for its known ligand-centered reductions, demonstrated that the transfer of $2e^{-}$ and $1H^{+}$ to the initial $[(TPP)Zn^{II}]$ complex yields the phlorin anion $[H(\bullet TPP)Zn^{II}]^{-}$. Its UV/Vis signature depicted two notable features, a Soret band located at 457 nm and a wide band peaking at 825 nm. Based on these spectroscopic signature, we propose that the band at 858 nm in our spectrum of $[(\bullet\bullet pTMA)Fe^{II}]^{2+}$ under CO indicates the formation of a phlorin anion following the net equation (1):

$$[(\bullet\bullet pTMA)Fe^{II}]^{2+} + H^{+} + CO \rightleftharpoons [H(\bullet pTMA)Fe^{II}–CO]^{3+} \quad (1)$$

Protons originate from residual water present in the DMF (typically 15 mM[51]). In the discussion above, we have demonstrated that $[(pTMA)Fe^{I}]^{3+}$ was unlikely to be carbonylated. We further propose that $[(\bullet\bullet pTMA)Fe^{II}]^{2+}$ is sequentially protonated to $[H(\bullet pTMA)Fe^{II}]^{3+}$ followed by carbonylation to finally afford $[H(\bullet pTMA)Fe^{II}–CO]^{3+}$.

The phlorin anion $[H(\bullet pTMA)Fe^{II}–CO]^{3+}$ (Scheme 3) has thus been characterized by a FTIR band located at

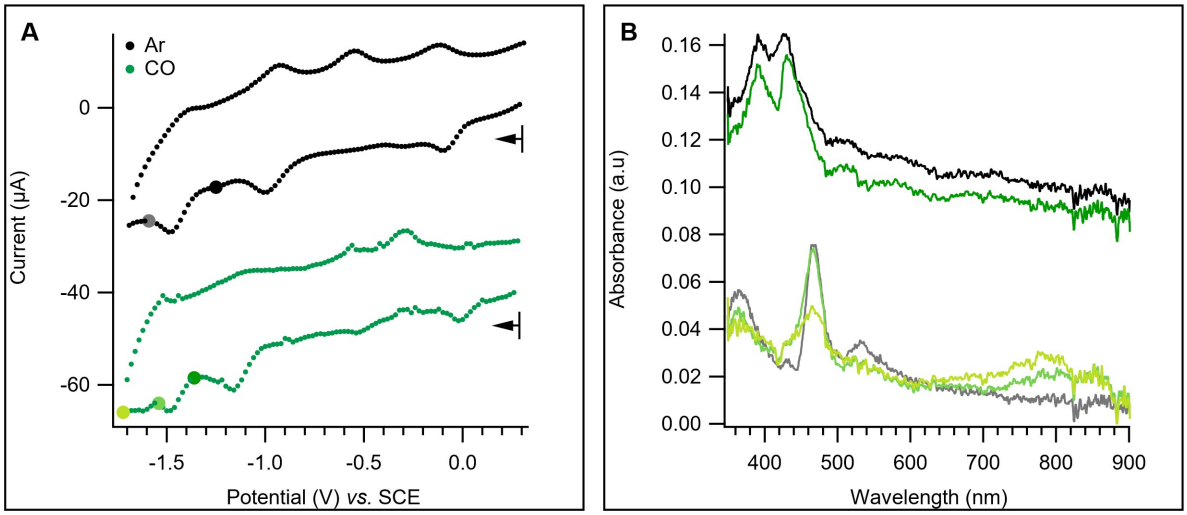

Figure 4. UV/Vis SEC under Ar atmosphere (black) or 3 bars P_{CO} (green), $[(pTMA)Fe^{III}–Cl]^{4+}$ 0.5 mM in DMF/0.1 M $TBAPF_6$. A: CV recorded during the SEC experiments, scan rate 20 mV/s. B: UV/Vis spectra being recorded in the meantime. (Black) Under Ar at −1.35 V *vs.* SCE. (Dark green) Under CO at −1.35 V *vs.* SCE. (Grey) Under Ar at −1.55 V *vs.* SCE. (Light green) Under CO at −1.55 V *vs.* SCE. (yellow) Under CO at −1.7 V *vs.* SCE.

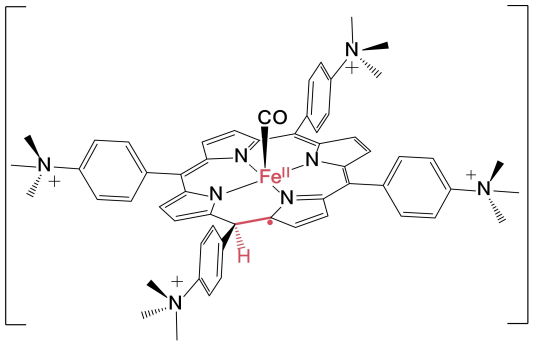

Scheme 3. Structure of the CO-coordinated phlorin anion [H-(•pTMA)Fe^{II}–CO]$^{3+}$.

1925 cm^{-1} and a UV/Vis absorption in the range 800–900 nm. It could be further reduced as suggested by three different observations. First, CV performed at low scan rate (20 mV/s) showed the presence of a fourth reduction wave around −1.6 V *vs.* SCE under CO atmosphere and not under Ar atmosphere (Figure 4, black CV under Ar, green CV under CO). This wave only appeared under CO atmosphere at low scan rate, indicative of the slow formation of [H(•pTMA)Fe^{II}–CO]$^{3+}$. A detailed study by cyclic voltammetry of this ECE process is provided in the Supporting Information (Figure S2B). Second, an additional weaker FTIR band (1878 cm^{-1}, Figure 3) started to grow passing this fourth reduction wave, indicating the presence of a new Fe–CO intermediate at the expense of the 1925 cm^{-1} related species. To get a more detailed view, we conducted FTIR potential step experiments to follow the evolution of the associated bands under CO atmosphere (Figure S12). Third, UV/Vis SEC depicted the appearance of an additional band around 790 nm (Figure 4, light green line) passing the fourth reduction wave. According to studies carried out with [(TPP)Zn^{II}], this species is likely the analog to the phlorin dianion [H(••TPP)Zn^{II}]$^{2-}$, pointing to the reduction of the CO-coordinated phlorin anion (1925 cm^{-1}) to the CO-coordinated phlorin dianion (1878 cm^{-1}), along reaction (2):

$$[H(\bullet pTMA)Fe^{II}-CO]^{3+} + e^- \rightleftharpoons [H(\bullet\bullet pTMA)Fe^{II}-CO]^{2+} \quad (2)$$

Resting State of (pTMA)Fe Species During Catalysis

FTIR SEC under CO_2 atmosphere allowed monitoring of Fe–CO species which are involved in the catalytic cycle and formation of side reaction products. However, the spectral window of FTIR SEC is only able to detect Fe–CO species. In order to obtain more information on non-carbonyl species involved in the mechanism, we conducted UV/Vis SEC under operando conditions. In a CO_2-saturated DMF/$TBAPF_6$ 0.1 M solution, CVs were recorded at 20 mV/s while UV/Vis spectra were collected. CV recorded during UV/Vis SEC under CO_2 (Figure 5, blue trace) was similar to that observed during FTIR SEC (Figure 2). It showed a catalytic current starting at ca. −1.3 V *vs.* SCE and the reverse scan appeared featureless. The fact that the expected re-oxidation wave of Fe–CO species formed during catalysis was not observed can be rationalized by carbonate (CO_3^{2-}) deposition at the electrode surface resulting in significant blocking of interfacial electron transfer.[38] In the absence of exogenous proton source, carbonate formation is known to result from the reaction between two CO_2 molecules, one CO_2 being bound to the catalyst and the other one acting as a Lewis acid, following reaction (3):[12]

$$[(pTMA)Fe^{II}-CO_2]^{2+} + CO_2 = [(pTMA)Fe^{II}-CO]^{4+} + CO_3^{2-} \quad (3)$$

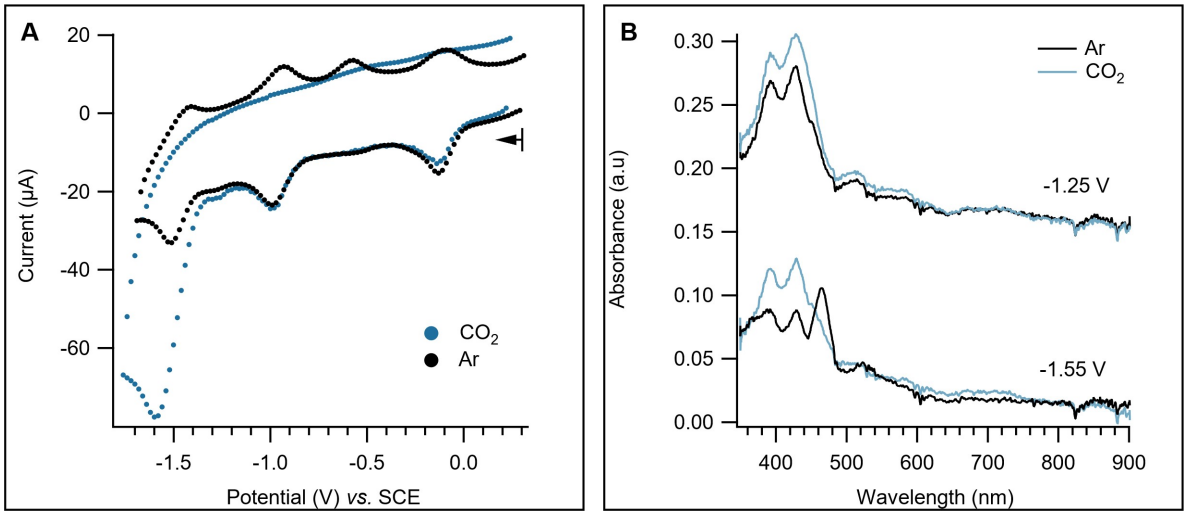

Figure 5. A: Cyclic voltammograms of [(pTMA)Fe^{III}–Cl]$^{4+}$ (0.5 mM) in DMF/0.1 M $TBAPF_6$ under Ar (black) and 3 bars P_{CO2} (blue) while scanning the potential at 20 mV/s. B: UV/Vis spectra being recorded in the meantime. Top: At −1.25 V *vs.* SCE under Ar (black) or CO_2 (blue). Bottom: At −1.55 V *vs.* SCE under Ar (black) or CO_2 (blue).

The carbonate formation was further evidenced by a significant shift of the baseline of the UV/Vis spectra recorded during catalysis (Figure S13). The spectra recorded at E = −1.25 V *vs.* SCE displayed the signature of a $[(pTMA)Fe^{I}]^{3+}$ species as demonstrated by the reference spectrum recorded under Ar atmosphere at the Fe^{I} level (Figure 1).

Under catalytic CO_2 reduction condition at E = −1.55 V *vs.* SCE, there were no noticeable differences between the spectrum obtained and that of $[(pTMA)Fe^{I}]^{3+}$. It strongly suggests that the resting state species during catalytic CO_2 reduction is $[(pTMA)Fe^{I}]^{3+}$. For comparison, a spectrum was recorded under Ar atmosphere in the absence of catalytic process at the same potential (−1.55 V *vs.* SCE). The spectrum depicted some features relative to both $[(pTMA)Fe^{I}]^{3+}$ (Soret bands at 392 and 425 nm) and $[(pTMA)Fe^{0}]^{2+}$ (Soret band and 467 nm) species.

Our operando UV/Vis SEC experiments revealed that $[(pTMA)Fe^{I}]^{3+}$ is the main species observed in the thin-film during electrocatalytic CO_2 reduction to CO. This is consistent with observations from FTIR SEC where no observable Fe–CO species are formed during early phase of the catalytic reduction. This can be rationalized by the decarbonylation step described in the catalytic mechanism (Scheme 2) where reduction of $[(pTMA)Fe^{II}–CO]^{4+}$ (directly at the electrode or through synproportionation reaction with $[(pTMA)Fe^{0}]^{2+}$) to form $[(pTMA)Fe^{I}]^{3+}$ with the release CO. These results are in agreement with a study by Costentin *et al.* reporting the catalytic activity of (TPP)Fe for CO_2 reduction to CO by UV/Vis SEC with $[(TPP)Fe^{I}]^{-}$ being the predominant steady state species at catalytic potentials.[34]

Towards a Complete Reaction Mechanism

The combination of FTIR and UV/Vis SEC enabled to draw a detailed mechanism for CO_2 electroreduction to CO catalyzed by $[(pTMA)Fe^{III}–Cl]^{4+}$ in DMF/TBAPF$_6$ (Scheme 4). After a three-electron reduction process generating the catalytically active species ($[(\bullet\bullet pTMA)Fe^{II}]^{2+}$ ↔$[(pTMA)Fe^{0}]^{2+}$), the latter can react with CO_2 leading to the putative $[(\bullet\bullet pTMA)Fe^{II}–CO_2]^{2+}$ intermediate (step *a*). Another molecule of CO_2 acting as Lewis acid triggers C–O bond cleavage leading to the generation of carbonate CO_3^{2-} and $[(pTMA)Fe^{II}–CO]^{4+}$ (step *b*). As the latter was detected by our FTIR SEC experiments under CO_2, we expect a small fraction of $[(pTMA)Fe^{II}–CO]^{4+}$ to diffuse away from the electrode surface to the bulk of the film and the remaining species to be reduced to $[(pTMA)Fe^{I}–CO]^{3+}$ (step *c*) either by reaction with another $[(pTMA)Fe^{0}]^{2+}$ molecule or by transfer of one electron from the electrode. This reduction process is followed by the loss of the CO ligand from the $[(pTMA)Fe^{I}]^{3+}$ coordination sphere (step *d*). This decarbonylation reaction is clearly demonstrated by the FTIR SEC studies under CO described above and by the observation of $[(pTMA)Fe^{I}]^{3+}$ by UV/Vis SEC under catalytic CO_2 turnover conditions. Finally, the catalytically active species $[(pTMA)Fe^{0}]^{2+}$ (↔$[(\bullet\bullet pTMA)Fe^{II}]^{2+}$) is re-generated by the one-electron reduction of $[(pTMA)Fe^{I}]^{3+}$ (step *e*).

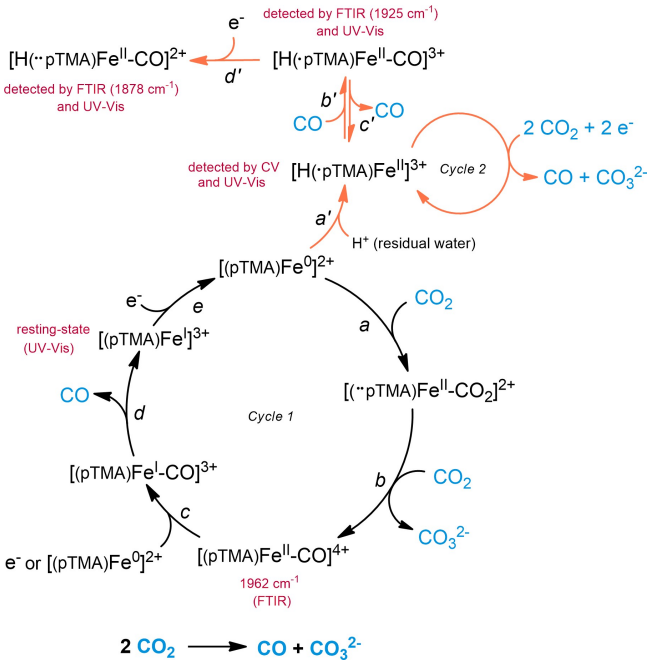

Scheme 4. Proposed detailed mechanism for CO_2 electrochemical reduction to CO with $[(pTMA)Fe^{III}–Cl]^{4+}$ catalyst.

A CO molecule was produced upon the first full completion of the catalytic cycle. Therefore, there is a competition between the binding of CO_2 or CO to $[(\bullet\bullet pTMA)Fe^{II}]^{2+}$ species. If CO_2 binds to $[(\bullet\bullet pTMA)Fe^{II}]^{2+}$, catalysis continues (*Cycle 1*). However, we demonstrated that $[(\bullet\bullet pTMA)Fe^{II}]^{2+}$ could also bind CO along with the transfer of one proton to the ligand to form the phlorin anion $[H(\bullet pTMA)Fe^{II}]^{3+}$ (step *a'*), leading to the CO-coordinated phlorin anion $[H(\bullet pTMA)Fe^{II}–CO]^{3+}$ (step *b'*), detected in both FTIR and UV/Vis SEC experiments. This species is in equilibrium with the phlorin anion $[H(\bullet pTMA)Fe^{II}]^{3+}$ (steps *b'–c'*), which existence is supported by both CV and UV/Vis SEC studies. This $[H(\bullet pTMA)Fe^{II}]^{3+}$ species and the catalytically active $[(\bullet\bullet pTMA)Fe^{II}]^{2+}$ species are identical except for the ligand's protonation. Since most of previously reported studies, done in the presence of large concentrations of proton donors, have led to significant TON values,[42,43] we speculated that $[H(\bullet pTMA)Fe^{II}]^{3+}$ could also act as a competent catalyst towards CO_2 reduction (Scheme 4, *Cycle 2*). The potential catalytic activity of $[H(\bullet pTMA)Fe^{II}]^{3+}$ was investigated by electrogenerating the latter under Ar atmosphere in the presence of one equivalent of water in our conventional setup (Figure S11). After saturation of a DMF + 0.1 M TBAPF$_6$ solution with CO_2 and addition of 250 equivalents of phenol as proton source, followed by a CPE at E = −1.6 V *vs.* SCE for 1 h, the phlorin species yielded 100 % FE_{CO} (TON_{CO} = 16). This performance is comparable to that of the native porphyrin species, which furnished 100 % FE_{CO} (TON_{CO} = 23) in the same conditions.

With the observation of CO coordination to highly reduced species $[H(\bullet pTMA)Fe^{II}–CO]^{3+}$ phlorin anion and $[H(\bullet\bullet pTMA)Fe^{II}–CO]^{2+}$ phlorin dianion (step *d'*), it is worthwhile to explore if CO can be further reduced. We thus performed CPE under 1 bar CO atmosphere in DMF/0.1 M $TBPAF_6$ with ethanol as proton source. The only gaseous or liquid product detected was methane (CH_4) with up to 18 % FE. A detailed description is given in Supporting Information (Figure S14–S16). Repeating the experiment under ^{13}CO showed that the CH_4 did not come from the reduction of CO but rather from the hydrolysis of the methyl groups of the TMA moieties. These results call for reassessment of a recent study reporting CO_2 electroreduction to CH_4 with homogeneous $[(pTMA)Fe^{III}–Cl]^{4+}$ in aqueous conditions,[36] in which no labelled experiments has been performed.[52]

Conclusion

UV/Vis SEC study demonstrated that $[(pTMA)Fe^{I}]^{3+}$ species is the resting state, *i.e.* the dominant species of the high-pressure CO_2 electroreduction to CO in thin-film. Thanks to the sensitivity of FTIR SEC the existence of two carbonyl species $[(pTMA)Fe^{II}–CO]^{4+}$ and $[H(\bullet pTMA)Fe^{II}–CO]^{3+}$ formed were revealed at catalytic potential upon longer times. The latter was shown to result from the existence of a secondary pathway involving the protonation of the porphyrin ligand into a phlorin ligand at the Fe^0 level and further coordination to CO.

These findings shed further light on the reasons for high selectivity towards CO production. As shown by our results and previous literature data, binding of CO_2 to Fe at the $[(pTMA)Fe^{0}]^{2+}$ level is favored over H^+ binding. However, $[(pTMA)Fe^{0}]^{2+}$ could be protonated at the ligand to yield phlorin species (Scheme 4, step *a'*). During prolonged electrolysis, CO accumulates at the electrode surface and in the bulk solution, increasingly promoting the secondary phlorin pathway (Scheme 4). It additionally raises the question of whether or not $[H(\bullet pTMA)Fe^{II}]^{3+}$ is active in reducing CO_2 to CO, since $[(pTMA)Fe^{III}–Cl]^{4+}$ used in long-term CPE has indeed demonstrated high Faradaic efficiencies towards CO over extended periods of time.[42,43] Our preliminary results indicated that $[H(\bullet pTMA)Fe^{II}]^{3+}$ phlorin anion exhibited similar activity towards CO_2RR as the activity of the $[(pTMA)Fe^{0}]^{2+}$ porphyrin (Scheme 4, *Cycle 2*). It raises the question of the true nature of the catalytically active species and prompts a deeper investigation of the catalytic activity of the phlorin anion. Such studies are underway and may open new perspectives for this class of highly active molecular CO_2 catalysts.

Supporting Information

The authors have cited additional references within the Supporting Information.[53,56]

Acknowledgements

A. S. acknowledges funding from the French government for her Ph.D. A. S. and E. A. M. acknowledge financial support from CNRS IEA. M. R. acknowledges partial financial support from Institut Universitaire de France (IUF). M. H. C. acknowledges financial support from Uppsala University.

Conflict of Interest

The authors declare no conflict of interest.

Data Availability Statement

The data that support the findings of this study are available from the corresponding author upon reasonable request.

Keywords: iron porphyrin · molecular catalysis · CO_2 reduction · mechanism · spectroelectrochemistry

[1] E. Boutin, M. Wang, J. C. Lin, M. Mesnage, D. Mendoza, B. Lassalle-Kaiser, C. Hahn, T. F. Jaramillo, M. Robert, *Angew. Chem. Int. Ed.* **2019**, *58*, 16172–16176.
[2] X. Ren, J. Zhao, X. Li, J. Shao, B. Pan, A. Salamé, E. Boutin, T. Groizard, S. Wang, J. Ding, X. Zhang, W.-Y. Huang, W.-J. Zeng, C. Liu, Y. Li, S.-F. Hung, Y. Huang, M. Robert, B. Liu, *Nat. Commun.* **2023**, *14*, 3401.
[3] Y. Wu, Z. Jiang, X. Lu, Y. Liang, H. Wang, *Nature* **2019**, *575*, 639–642.
[4] S.-T. Dong, C. Xu, B. Lassalle-Kaiser, *Chem. Sci.* **2023**, *14*, 550–556.
[5] M. Wang, K. Torbensen, D. Salvatore, S. Ren, D. Joulié, F. Dumoulin, D. Mendoza, B. Lassalle-Kaiser, U. Işci, C. P. Berlinguette, M. Robert, *Nat. Commun.* **2019**, *10*, 3602.
[6] E. Boutin, A. Salamé, L. Merakeb, T. Chatterjee, M. Robert, *Chem. Eur. J.* **2022**, *e202200697*.
[7] T. Yan, X. Chen, L. Kumari, J. Lin, M. Li, Q. Fan, H. Chi, T. J. Meyer, S. Zhang, X. Ma, *Chem. Rev.* **2023**, *123*, 10530–10583.
[8] Z. Liu, X. Lv, S. Kong, M. Liu, K. Liu, J. Zhang, B. Wu, Q. Zhang, Y. Tang, L. Qian, L. Zhang, G. Zheng, *Angew. Chem. Int. Ed.* **2023**, e202309319.
[9] R. E. Vos, K. E. Kolmeijer, T. S. Jacobs, W. Van der Stam, B. M. Weckhuysen, M. T. M. Koper, *ACS Catal.* **2023**, 8080–8091.
[10] R. Francke, B. Schille, M. Roemelt, *Chem. Rev.* **2018**, *118*, 4631–4701.
[11] N. W. Kinzel, C. Werlé, W. Leitner, *Angew. Chem. Int. Ed.* **2021**, *60*, 11628–11686.
[12] M. Hammouche, D. Lexa, J. M. Savéant, M. Momenteau, *J. Electroanal. Chem. Interfacial Electrochem.* **1988**, *249*, 347–351.
[13] M. Hammouche, D. Lexa, M. Momenteau, J. M. Savéant, *J. Am. Chem. Soc.* **1991**, *113*, 8455–8466.
[14] I. Bhugun, D. Lexa, J.-M. Savéant, *J. Am. Chem. Soc.* **1996**, *118*, 1769–1776.
[15] C. Costentin, S. Drouet, M. Robert, J.-M. Savéant, *Science* **2012**, *338*, 90–94.
[16] P. Gotico, B. Boitrel, R. Guillot, M. Sircoglou, A. Quaranta, Z. Halime, W. Leibl, A. Aukauloo, *Angew. Chem. Int. Ed.* **2019**, *58*, 4504–4509.

[17] P. Gotico, L. Roupnel, R. Guillot, M. Sircoglou, W. Leibl, Z. Halime, A. Aukauloo, *Angew. Chem. Int. Ed.* **2020**, *59*, 22451–22455.
[18] J. Bonin, M. Chaussemier, M. Robert, M. Routier, *ChemCatChem* **2014**, *6*, 3200–3207.
[19] J. Grodkowski, D. Behar, P. Neta, P. Hambright, *J. Phys. Chem. A* **1997**, *101*, 248–254.
[20] T. Dhanasekaran, J. Grodkowski, P. Neta, P. Hambright, E. Fujita, *J. Phys. Chem. A* **1999**, *103*, 7742–7748.
[21] B. Mondal, A. Rana, P. Sen, A. Dey, *J. Am. Chem. Soc.* **2015**, *137*, 11214–11217.
[22] D. Lexa, M. Momenteau, J. Mispelter, *BBA* **1974**, *338*, 151–163.
[23] C. Gueutin, D. Lexa, *Electroanalysis* **1996**, *8*, 1029–1033.
[24] D. Motz, S. Praetz, C. Schlesiger, J. Henniges, F. Böttcher, B. Hesse, H. Castillo-Michel, S. Mijatz, W. Malzer, B. Kanngießer, C. Vogt, *J. Anal. At. Spectrom.* **2023**, *38*, 391–402.
[25] T. E. Westre, P. Kennepohl, J. G. DeWitt, B. Hedman, K. O. Hodgson, E. I. Solomon, *J. Am. Chem. Soc.* **1997**, *119*, 6297–6314.
[26] D. Mendoza, S. Dong, N. Kostopoulos, V. Pinty, O. Rivada-Wheelaghan, E. Anxolabéhère-Mallart, M. Robert, B. Lassalle-Kaiser, *ChemCatChem* **2023**, *15*, e202201298.
[27] M. Tarrago, S. Ye, F. Neese, *Chem. Sci.* **2022**, *13*, 10029–10047.
[28] H. Xu, Z. Fan, S. Zhu, M. Shao, *Curr. Opin. Electrochem.* **2023**, 101363.
[29] S. Amanullah, P. Saha, A. Dey, *J. Am. Chem. Soc.* **2021**, *143*, 13579–13592.
[30] D. Mendoza, S.-T. Dong, B. Lassalle-Kaiser, *COCIS* **2022**, *61*, 101635.
[31] C. Costentin, J.-M. Savéant, C. Tard, *Proc. Natl. Acad. Sci. USA* **2018**, *115*, 9104–9109.
[32] C. Römelt, S. Ye, E. Bill, T. Weyhermüller, M. van Gastel, F. Neese, *Inorg. Chem.* **2018**, *57*, 2141–2148.
[33] C. Costentin, J.-M. Savéant, *ACS Catal.* **2018**, *8*, 5286–5297.
[34] R. Deeba, A. Collard, C. Rollin, F. Molton, S. Chardon-Noblat, C. Costentin, *ChemElectroChem* **2023**, e202300350.
[35] A. R. Ramuglia, M. Göbel, V. Budhija, M. Werheid, K. H. Ly, M. Schwalbe, I. M. Weidinger, *Inorg. Chem.* **2023**, *62*, 10232–10240.
[36] Y. Li, S. Xie, X. Huang, W. Song, C. Chen, H. Sheng, J. Zhao, *App. Catal. B* **2023**, *329*, 122542.
[37] E. Anxolabéhère-Mallart, G. Chottard, D. Lexa, *New J. Chem.* **1994**, *18*, 889–899.
[38] C. Costentin, S. Drouet, G. Passard, M. Robert, J.-M. Savéant, *J. Am. Chem. Soc.* **2013**, *135*, 9023–9031.
[39] H. Rao, J. Bonin, M. Robert, *Chem. Commun.* **2017**, *53*, 2830–2833.
[40] H. Rao, C.-H. Lim, J. Bonin, G. M. Miyake, M. Robert, *J. Am. Chem. Soc.* **2018**, *140*, 17830–17834.
[41] H. Rao, J. Bonin, M. Robert, *ChemSusChem* **2017**, *10*, 4447–4450.
[42] I. Azcarate, C. Costentin, M. Robert, J.-M. Savéant, *J. Am. Chem. Soc.* **2016**, *138*, 16639–16644.
[43] C. Costentin, M. Robert, J.-M. Savéant, A. Tatin, *Proc. Natl. Acad. Sci. USA* **2015**, *112*, 6882–6886.
[44] S. J. Borg, S. P. Best, *J. Electroanal. Chem.* **2002**, *535*, 57–64.
[45] F. Paulat, N. Lehnert, *Inorg. Chem.* **2008**, *47*, 4963–4976.
[46] C. De Silva, K. Czarnecki, M. D. Ryan, *Inorg. Chim. Acta* **1999**, *287*, 21–26.
[47] N. H. Mitchell, N. Elgrishi, *J. Phys. Chem. C* **2023**, *127*, 10938–10946.
[48] J. G. Lanese, G. S. Wilson, *J. Electrochem. Soc.* **1972**, *119*, 1039.
[49] G. S. Wilson, Gerald. Peychal-Heiling, *Anal. Chem.* **1971**, *43*, 550–556.
[50] G. S. Wilson, Gerald. Peychal-Heiling, *Anal. Chem.* **1971**, *43*, 545–550.
[51] M. L. Pegis, D. J. Martin, C. F. Wise, A. C. Brezny, S. I. Johnson, L. E. Johnson, N. Kumar, S. Raugei, J. M. Mayer, *J. Am. Chem. Soc.* **2019**, *141*, 8315–8326.
[52] B. Seger, M. Robert, F. Jiao, *Nat. Sustain.* **2023**, *6*, 236–238.
[53] D. Lexa, P. Rentien, *J. Electroanal. Chem.* **1985**, *191*, 253–279.
[54] G. Balducci, G. Chottard, C. Gueutin, D. Lexa, J.-M. Savéant, *Inorg. Chem.* **1994**, *33*, 1972–1978.
[55] K. W. Kwong, D. Patel, J. Malone, N. F. Lee, B. Kash, R. Zhang, *New J. Chem.* **2017**, *41*, 14334–14341.
[56] K. M. Kadish, G. Larson, D. Lexa, M. Momenteau, *J. Am. Chem. Soc.* **1975**, *97*, 282–288.

Manuscript received: July 2, 2024
Accepted manuscript online: August 19, 2024
Version of record online: October 18, 2024